

Position tracking and attitude control for quadrotors via active disturbance rejection control method

Yuan YUAN^{1*}, Lei CHENG², Zidong WANG¹ & Chong SUN²

¹*Department of Computer Science, Brunel University London, Uxbridge UB8 3PH, UK;*

²*School of Astronautics, Northwestern Polytechnical University, Xi'an 710072, China*

Received 4 July 2018/Accepted 19 July 2018/Published online 19 December 2018

Abstract In this paper, a trigonometric-saturation-function-based position controller is designed for the quadrotor system with internal and external disturbances. Furthermore, in the attitude control problem, a dual closed-loop structure is put forward. Specifically, a nonlinear extended-state-observer (ESO) is employed to provide an estimate for the so-called total disturbance. Then, based on the estimate provided by the ESO, a nonlinear composite control strategy is designed for the purpose of angular tracking. Some sufficient conditions are established to guarantee that the position and attitude subsystems are stable. The contributions are mainly as follows. (1) A trigonometric-saturation-function is used in the position control which could guarantee that the studied system is fully-actuated. (2) The nonlinear ESO is implemented in the attitude control-loop which could enhance the anti-disturbance property. Finally, some numerical simulations and practical experiments are provided to verify the applicability of the proposed methodology.

Keywords position control, quadrotor system, extended-state-observer, attitude control

Citation Yuan Y, Cheng L, Wang Z D, et al. Position tracking and attitude control for quadrotors via active disturbance rejection control method. *Sci China Inf Sci*, 2019, 62(1): 010201, <https://doi.org/10.1007/s11432-018-9548-5>

1 Introduction

In recent years, the unmanned aerial vehicles (UAVs) have gained great attention owing to their distinguishing advantages over the ground robots to perform a desired task in the dangerous environment [1]. More recently, a growing interest in UAVs has been witnessed in the research community [2–4]. Among the various UAVs, the quadrotor platform has been widely applied in path-following and landing maneuver [5, 6]. A number of researchers have been focusing on the position control problem of the quadrotor system. To be more specific, an adaptive switching supervisory controller has been used in position trajectory-tracking in [7]. In [8], an inner-outer loop control structure has been proposed in the position control problem of a quadrotor with state and input constraints. In [9], a double-integral-observer-based nonlinear tracking control scheme has been designed for a quadrotor. In [10, 11], novel control schemes have been proposed for the purpose of handling the disturbances. In [12], a smooth curve tracking algorithm has been designed such that the quadrotor is capable of tracking a desired trajectory under a constant wind disturbance. In [13], a two-time-scaled tracking control strategy has been studied which could handle disturbances in multi-UAV. In [14], a virtual attitude dynamic surface control strategy has been developed which could deal with the unmatched disturbances and unknown dynamics in the flying vehicle. In [15], a nonlinear disturbance-observer-based position tracking control scheme has been put forward to track a desired position subjected to disturbances for electrohydraulic actuators.

* Corresponding author (email: snowkey@aliyun.com)

In engineering practice, the attitude control of the quadrotor is also very importance because it maintains the vehicle in a desired orientation and attitude. In [16], the position of the quadrotor has been controlled by a remote controller via the wireless communication channel, while its attitude has been stabilized via an onboard microprocessor. In [17], a novel quaternion-based feedback control scheme has been proposed for exponential attitude stabilization of a quadrotor with vertical takeoff and landing. In [18], a distributed finite-time attitude containment controller has been proposed to achieve the goal of attitude regulation in the finite time. In [19], a multivariable attitude control law has been developed, which could drive the attitude tracking error to zero in finite time. In [20], to accelerate the response speed of the attitude control loop, a finite-time controller has been designed. A robust attitude stabilization controller has been proposed which consists of a nominal state-feedback controller and a robust compensator [21]. Among all the attitude control schemes, it should be pointed out that the active disturbance rejection control (ADRC) method has had its own merits in anti-interference performance and does not require the accurate math model [22, 23]. Generally, the ADRC has consisted of three part, namely, the tracking differentiator, the extended-state-observer (ESO) and the nonlinear feedback controller [24–27]. Notice that it is an appropriate method to control quadrotor attitude systems for the reason that the ESO has had an inherent decoupling function [28]. Very recently, some pioneering research papers have been carrying out the attitude control of quadrotors using ADRC [29].

It is worth mentioning that the position and attitude control of the quadrotors are coupled and should be addressed at the same time. Nevertheless, the corresponding results are really scattered, which formulates one of the main motivations of writing the current paper. As such, it is necessary and significant to carry out the position and attitude control of the quadrotors simultaneously using the ADRC with a trigonometric saturation function.

Notations. In this paper, $|\cdot|$ denotes the absolute value. For any matrix A , A^T denotes the transpose of the matrix A . $\text{fal}(\cdot)$ is a nonlinear function as follows:

$$\text{fal}(e(t), \alpha, \delta) = \begin{cases} \frac{e(t)}{\delta^{1-\alpha}}, & |e(t)| \leq \delta, \\ |e(t)|^\alpha \text{sign}(e(t)), & |e(t)| > \delta, \end{cases}$$

where $e(t)$ is a variable, and $\alpha \in (0, 1)$ and δ are two given parameters. $\text{fal}(\cdot)$ is a piecewise function.

2 Dynamic model of quadrotor

According to [17], the dynamic model of a quadrotor is

$$\ddot{x}(t) = (\sin(\theta(t)) \cos(\phi(t)) \cos(\Psi(t)) + \sin(\Psi(t)) \sin(\phi(t)))u_1(t), \tag{1}$$

$$\ddot{y}(t) = (\sin(\theta(t)) \cos(\phi(t)) \sin(\Psi(t)) - \cos(\Psi(t)) \sin(\phi(t)))u_1(t), \tag{2}$$

$$\ddot{z}(t) = (\cos(\theta(t)) \cos(\phi(t)))u_1(t) - g, \tag{3}$$

$$\ddot{\phi}(t) = u_2(t) + (-I_R \dot{\theta}(t)(-\Omega_1(t) + \Omega_2(t) - \Omega_3(t) + \Omega_4(t)) + \dot{\theta}(t)\dot{\Psi}(t)(I_y - I_z))/I_x, \tag{4}$$

$$\ddot{\theta}(t) = u_3(t) + (I_R \dot{\phi}(t)(-\Omega_1(t) + \Omega_2(t) - \Omega_3(t) + \Omega_4(t)) + \dot{\phi}(t)\dot{\Psi}(t)(I_z - I_x))/I_y, \tag{5}$$

$$\ddot{\Psi}(t) = u_4(t) + (\dot{\phi}(t)\dot{\theta}(t)(I_x - I_y))/I_z, \tag{6}$$

where I_x , I_y and I_z denote three principal moments of inertia in axial direction; body mass and gravitational acceleration are denoted by m and g under earth fixed inertial frame, respectively; $\Omega_j(t)$, $j = 1, 2, 3, 4$ represent rotational speeds of four propellers; I_R is the propeller rotational inertia rotating the corresponding motor axes; $(\phi(t), \theta(t), \Psi(t))^T$ denotes the Euler angle vector of a quadrotor rotating around three axes. Note that the aforementioned physical quantities are defined in the earth-fixed inertial frame; Let $u_1(t) = F_{VT}(t)/m$, $u_2(t) = M_1(t)/I_x$, $u_3(t) = M_2(t)/I_y$ and $u_4(t) = M_3(t)/I_z$; $F_{VT}(t)$ represents the lift force; $M_1(t)$, $M_2(t)$ and $M_3(t)$ denote the driving torques of roll, pitch and yaw axis, respectively. The schematic diagram of control is shown as Figure 1. In Figure 1, the target attitude angles are calculated by the position controller and the basic throttle control $u_1(t)$ is generated

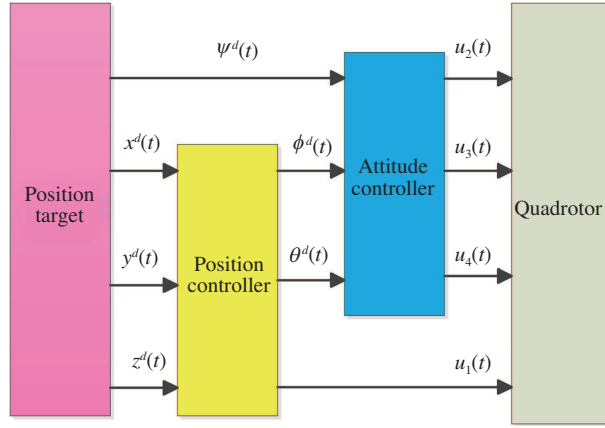


Figure 1 (Color online) The schematic diagram of control.

by the position controller. $u_2(t)$, $u_3(t)$ and $u_4(t)$ are generated by the attitude controller. Attitude angle torques are acquired as a superposition of three throttle increments and basic throttle control. Then, the attitude angle torques are assigned to four brushless DC motors.

3 Design of positioning subsystem controller

We can begin with the dynamics of the position (1)–(3). Take the x direction as an example. Let

$$\begin{aligned} x(t) &= x_1(t), \quad \dot{x}(t) = x_2(t), \quad \ddot{x}(t) = \tau_1(t), \\ \tilde{x}_1(t) &= x_1(t) - x^d(t), \quad \tilde{x}_2(t) = x_2(t) - \dot{x}^d(t), \end{aligned}$$

where $\tilde{x}_1(t)$ (respectively, $\tilde{x}_2(t)$) denotes the error between the current position (respectively, translational velocity) and the target position (respectively, target translational velocity). We could obtain the x position error system as follows:

$$\dot{\tilde{x}}_1(t) = \tilde{x}_2(t), \tag{7}$$

$$\dot{\tilde{x}}_2(t) = \tau_1(t) - \dot{x}^d(t). \tag{8}$$

In the x position subsystem (1), we introduce the virtue control law $\tau_1(t)$ as follows:

$$\tau_1(t) = -m_1 \arctan(k_1 \tilde{x}_1(t) + l_1 \tilde{x}_2(t)) - n_1 \arctan(l_1 \tilde{x}_2(t)) + \dot{x}^d(t), \tag{9}$$

where m_1 , k_1 , l_1 and n_1 are four positive parameters to be adjusted. In the following, the sufficient condition is provided to guarantee that the error system (7) and (8) is stable by using the virtual control law (9).

Theorem 1. Consider the error system (7) and (8) with the virtual control law (9). If there exist four appropriate coefficients m_1 , k_1 , l_1 and n_1 satisfying

$$m_1 > 0, \quad k_1 > 0, \quad l_1 > 0, \quad n_1 > 0,$$

then the error system (7) and (8) is stable.

Proof. For $\Delta \arctan(\Delta) - \frac{1}{2} \ln(1 + (\Delta)^2) \geq 0$, $\Delta \in \mathbb{R}$, we select the following Lyapunov function:

$$\begin{aligned} V_1(t) &= m_1 \left[(k_1 \tilde{x}_1(t) + l_1 \tilde{x}_2(t)) \arctan(k_1 \tilde{x}_1(t) + l_1 \tilde{x}_2(t)) - \frac{1}{2} \ln(1 + (k_1 \tilde{x}_1(t) + l_1 \tilde{x}_2(t))^2) \right] \\ &\quad + n_1 \left[l_1 \tilde{x}_2(t) \arctan(l_1 \tilde{x}_2(t)) - \frac{1}{2} \ln(1 + (l_1 \tilde{x}_2(t))^2) \right] + \frac{1}{2} k_1 \tilde{x}_2^2(t). \end{aligned}$$

Taking the derivative of $V_1(t)$ along (9), we have

$$\begin{aligned} \dot{V}_1(t) &= m_1(k_1\dot{\tilde{x}}_1(t) + l_1\dot{\tilde{x}}_2(t)) \arctan(k_1\tilde{x}_1(t) + l_1\tilde{x}_2(t)) + n_1l_1\tilde{x}_2(t) \arctan(l_1\dot{\tilde{x}}_2(t)) + k_1\tilde{x}_2(t)\dot{\tilde{x}}_2(t) \\ &= -l_1[m_1 \arctan(k_1\tilde{x}_1(t) + l_1\tilde{x}_2(t)) + n_1 \arctan(l_1\tilde{x}_2(t))]^2 - k_1n_1\tilde{x}_2(t) \arctan(l_1\tilde{x}_2(t)) \\ &< 0. \end{aligned}$$

The proof is complete.

In the same vain, the virtual control laws for the y position subsystem (2) and z position subsystem (3) are designed as

$$\tau_2(t) = -m_2 \arctan(k_2\tilde{y}_1(t) + l_2\tilde{y}_2(t)) - n_2 \arctan(l_2\tilde{y}_2(t)) + \dot{y}^d(t). \quad (10)$$

For $u_1^2(t) = \tau_1^2(t) + \tau_2^2(t) + (\ddot{z}(t) + g)^2$, the target roll angle and target pitch angle can be obtained from (1)–(3) as

$$\phi^d(t) = \arcsin\left(\frac{\tau_1(t) \sin(\Psi^d(t)) - \tau_2(t) \cos(\Psi^d(t))}{u_1(t)}\right), \quad (11)$$

and

$$\theta^d(t) = \arctan\left(\frac{\tau_1(t) \cos(\Psi^d(t)) + \tau_2(t) \sin(\Psi^d(t))}{u_1(t) \cos(\phi^d(t))}\right), \quad (12)$$

respectively. In the position control, $u_1(t)$ is generated by an independent altitude controller. Then, the target angles $\phi^d(t)$, $\theta^d(t)$ and $\Psi^d(t)$ are fed into attitude controller. It follows from (11) and (12) that the under-actuated case $\phi^d(t) = \theta^d(t) = \pi/2$ could be circumvented.

4 Design of attitude subsystem controller

4.1 Design of inner loop controller

In virtue of the ADRC method, an inner loop controller has been proposed to keep track of the target angular velocity. Without loss of generality, we only take consideration of the control around the roll axis. In the dynamic model of the roll axis (4), we define

$$\begin{aligned} M_1(t)/I_x &= b_0u_2(t) + \Delta u_2(t), \\ f(t) &= \Delta u_2(t) + [-I_R\dot{\theta}(t)(-\Omega_1(t) + \Omega_2(t) - \Omega_3(t) + \Omega_4(t)) + \dot{\theta}(t)\dot{\Psi}(t)(I_y - I_z)]/I_x, \end{aligned}$$

where b_0 is an estimated value of $1/I_x$; $u_2(t)$ represents the control input; $\Delta u_2(t)$ denotes the external disturbances; $f(t)$ is the nonlinear dynamics consisting of gyroscopic effects and coupling dynamics. By setting $\dot{\phi}(t) = x_1(t)$, it follows from (4) that

$$x_1(t) = f(t) + b_0u_2(t). \quad (13)$$

Note that b_0 is a constant in the first-order system and can be taken as an adjustable parameter.

4.1.1 Design of the ESO

In the quadrotor system, the ESO is employed to deal with the so-called total disturbance. Assume that $f(t)$ is continuously differentiable and bounded. We regard $f(t)$ as an extended state $x_2(t)$, i.e., $f(t) = x_2(t)$. Then, (13) becomes

$$\dot{x}_1(t) = x_2(t) + b_0u_2(t), \quad (14)$$

$$\dot{x}_2(t) = \omega(t), \quad (15)$$

where $\omega(t)$ is the derivative of $x_2(t)$. Note that $\omega(t)$ is bounded in practice. The ESO designed for system (4) takes the form as

$$\dot{z}_1(t) = z_2(t) - \beta_1 e_1(t) + b_0 u_2(t), \tag{16}$$

$$\dot{z}_2(t) = -\beta_2 \text{fal}(e_1(t), 0.5, \delta_1), \tag{17}$$

where $z_1(t)$ and $z_2(t)$ are estimates of $x_1(t)$ and $x_2(t)$, respectively; $e_1(t) = z_1(t) - x_1(t)$; β_1 and β_2 are two adjustable parameters. Notice that the segmentation points in $\text{fal}(\cdot)$ are non-differentiable points. For the purpose of theoretic analysis, we assign $\delta_1 = 0$ in (16) and (17), i.e., $\text{fal}(e(t), 0.5, 0) = |e(t)|^{\frac{1}{2}} \text{sign}(e(t))$. For simplicity, $\text{fal}(e_1(t), 0.5, 0)$ is indicated as $\text{fal}(e_1(t))$. In addition, we define $e_2(t) = z_2(t) - x_2(t)$. According to (14)–(17), the error system is shown as follows:

$$\dot{e}_1(t) = e_2(t) - \beta_1 e_1(t), \tag{18}$$

$$\dot{e}_2(t) = -\omega(t) - \beta_2 \text{fal}(e_1(t)). \tag{19}$$

According to [30], if there exist two appropriate positive coefficients β_1 and β_2 with $\beta_2 > \frac{3}{4}\beta_1^2$, then the ESO (16) and (17) for the system (14) and (15) is stable.

4.1.2 Nonlinear state error feedback controller

In order to track the target angular velocity signal from the outer loop, a nonlinear feedback controller is designed. Define $\zeta(t) = v(t) - z_1(t)$, where $v(t)$ is the given angular velocity; $z_1(t)$ represents the estimate of the angular velocity. The nonlinear feedback controller is designed as

$$u_2(t) = (\alpha_1 \text{fal}(\zeta(t), \sigma_1, \delta_2) - z_2(t))/b_0, \tag{20}$$

where α_1 is the parameter of the nonlinear controller; $z_2(t)/b_0$ is to compensate $f(t)$ in system (14) and (15). Define

$$s_1(t) = v(t) - x_1(t). \tag{21}$$

The derivative of $s_1(t)$ in (21) is given as

$$\dot{s}_1(t) = \dot{v}(t) - f(t) - b_0 \tilde{u}, \tag{22}$$

where $\dot{v}(t)$ is continuous and bounded. For simplicity, $\text{fal}(\zeta(t), \sigma_1, \delta_2)$ is denoted by $\text{fal}(\zeta(t))$. According to (21), it is easy to get $\zeta(t) = s_1(t) - e_1(t)$. In addition, one has that $\dot{s}_1(t) = \dot{v}(t) - \alpha_1 \text{fal}(\zeta(t)) + e_2(t)$, where $e_2(t) = z_2(t) - f(t)$.

Theorem 2. Consider the closed-loop system (21) and (22) with the feedback controller (20). If there exists a positive parameter α_1 and an arbitrarily small positive constant ζ_0 satisfying

$$\alpha_1 > \frac{M_1}{\text{fal}(\zeta_0)}, \tag{23}$$

where $M_1 = \max\{|\dot{v}(t) + \beta_1 e_1(t)|\}$, for any $\zeta(t) \in (\zeta_0, +\infty)$, then the closed-loop system (21) and (22) is stable, that is, the output $x_1(t)$ could converge to input $v(t)$ by using controller (20).

Proof. Construct a Lyapunov function as

$$V_3(t) = \frac{1}{2}(s_1(t) - e_1(t))^2.$$

If (23) holds, the derivative of $V_3(t)$ is given as

$$\begin{aligned} \dot{V}_3(t) &= (s_1(t) - e_1(t))(\dot{v}(t) - \alpha_1 \text{fal}(\zeta(t)) + e_2(t) - (e_2(t) - \beta_1 e_1(t))) \\ &= -(s_1(t) - e_1(t))\alpha_1 \text{fal}(\zeta(t)) + (s_1(t) - e_1(t))(\dot{v}(t) + \beta_1 e_1(t)) \\ &\leq -(\zeta(t))\alpha_1 \text{fal}(\zeta(t)) + M_1 |\zeta(t)| \\ &< 0. \end{aligned}$$

The proof is complete.

Table 1 Parameters of the position controller

Parameter	Value	Parameter	Value
m_1	5.0	m_2	5.0
n_1	0.5	n_2	0.5
k_1	2.3	k_2	2.3
l_1	7.5	l_2	7.6

Table 2 Parameters of the attitude controller

Parameter	Roll	Pitch	Yaw
γ_1	1.4×10^3	1.4×10^3	1.3×10^3
γ_2	2.9×10^4	3.0×10^4	5.0×10^3
b_0	5.0×10^2	5.0×10^2	5.0×10^2
η_1	15.0	15.0	3.0
p	1.0	1.0	10.0
d	0.1	0.1	0.1

4.2 Design of outer loop controller

A PD controller is adopted as an outer loop control law

$$v(t) = k_p \left(\varepsilon(t) + T_D \frac{d\varepsilon(t)}{dt} \right), \quad (24)$$

where $\rho(t)$ is the target angle given by a remote controller, $\varepsilon(t)$ is an error between the target angle and quadrotor current angle. Note that $\varepsilon(t) = \rho(t) - y(t)$ holds. The output value in outer loop is the target value in inner loop.

Remark 1. It is not difficult to implement the proposed methodology in the control of the quadrotor because (1) in the design of the attitude controller, all the external and internal disturbances are estimated by the ESO and hence our method does not require the specific information of the quadrotor model; and (2) the design of the virtue control law is also independent of the system dynamics. As such, we could arrive at the the conclusion that, even if the system model of the quadrotor is different from (1)–(6), it is also easy to implement the proposed method.

5 Simulations and experiments

5.1 Simulations

In this subsection, some numerical simulations are carried out for the position tracking of the quadrotor. We assign $x^d(t) = 5 \sin(0.2t)$ m, $y^d(t) = -5 \cos(0.2t)$ m, $\Psi^d(t) = \arctan(y_1^d(t)/x_1^d(t)) + 0.5\pi$ rad and $T = 0.001$ s. The two-dimension simulation result is shown in Figure 2. In Figure 2, the quadrotor tracks a circle with radius of 5 m at the height of 5 m, which verifies the validity of the position controller (9) and (10) as well as the attitude controller (20) and (24). The parameters of the position controller (9) and (10) is provided in Table 1. In Table 1, the subscript numbers 1 and 2 represent the parameters associated with the roll axis and the pitch axis, respectively. The simulation results of the position controller (9) and (10) of the quadrotor are shown in Figure 3. The current position of the quadrotor is almost coincident with the given target position as shown in Figure 3(a) and (c). It is shown that the position error $(\tilde{x}_1(t), \tilde{y}_1(t))$ is no more that 0.02 m after 3 s in Figure 3(b) and (d). The virtual control laws $\tau_1(t)$ and $\tau_2(t)$ are capable of reversing the trend of corresponding position error. The parameters of the attitude controller (20) and (24) are provided in Table 2. In Table 2, both γ_i with $i = 1, 2$ and b_0 are parameters of ESO. η_1 is the parameter of the nonlinear feedback controller. p and d are parameters of the PD feedback. The simulation results of the attitude controller in (20) and (24) are shown in Figures 4–6. In Figures 4–6, the roll, pitch and yaw angles of quadrotor are capable of tracking the target angles (11) and (12), and $\Psi^d(t)$, respectively.

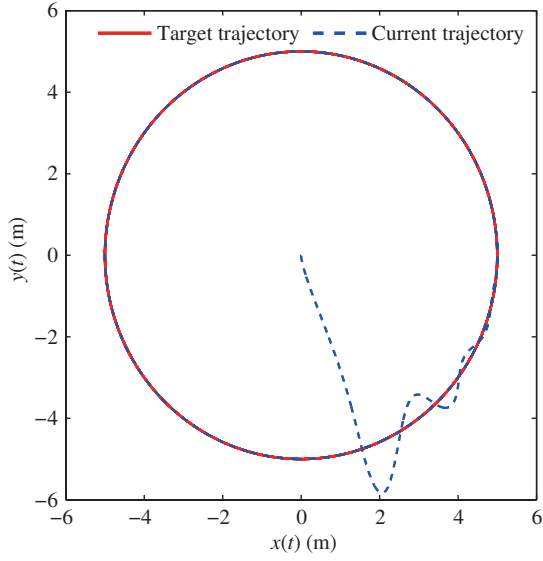


Figure 2 (Color online) The two-dimensional position simulation results of a quadrotor.

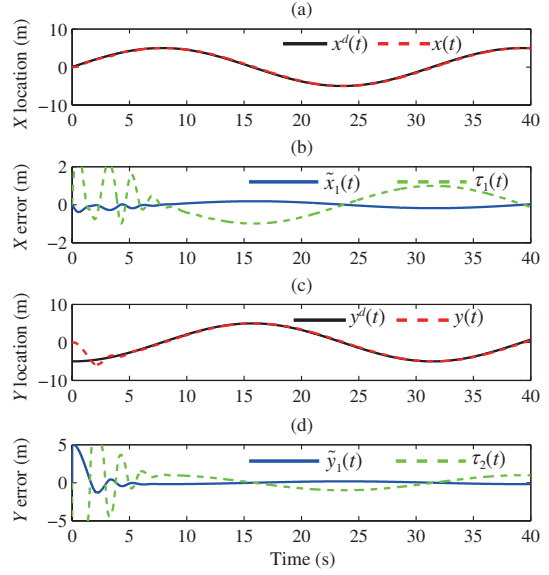


Figure 3 (Color online) The position simulation results. (a) x position; (b) x position error; (c) y position; (d) y position error.

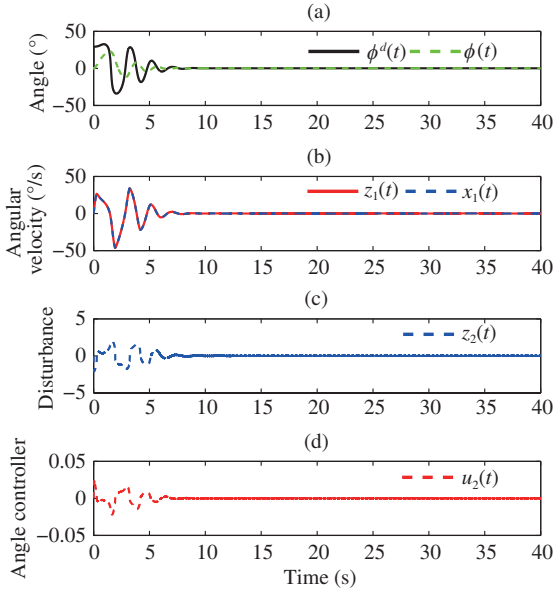


Figure 4 (Color online) Roll angle tracking results of two-dimensional position simulation. (a) Roll angle; (b) roll angular velocity; (c) roll angle disturbance estimation; (d) roll angle controller.

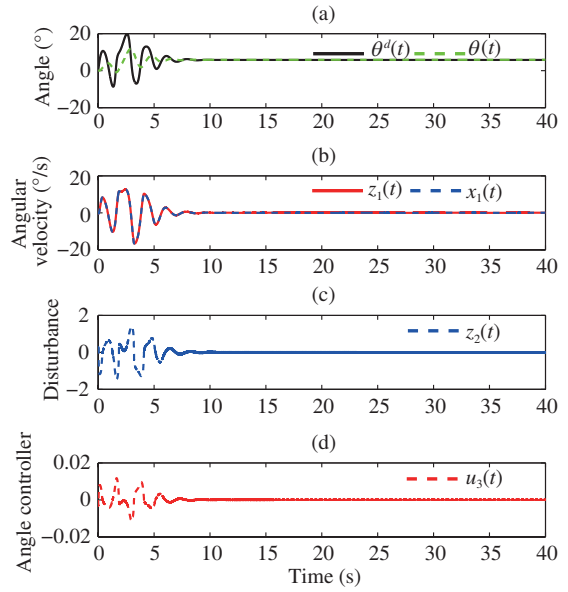


Figure 5 (Color online) Pitch angle tracking results of two-dimensional position simulation. (a) Pitch angle; (b) pitch angular velocity; (c) pitch angle disturbance estimation; (d) pitch angle controller.

5.2 Experiments

In this paper, a group of comparative experiments are carried out to illustrate the advantages of the proposed methodology over PID control method. The experimental quadrotor platform is shown in Figure 7. The target of position tracking control are set as $x^d(t) = 5 + 3 \sin(0.1t)$ m, $y^d(t) = 5 + 3 \cos(0.1t)$ m and $\Psi^d(t) = 0^\circ$. The sampling period is set as $T = 0.002$ s. Experimental results of trajectory tracking based on dual closed-loop PID attitude controller are shown in Figures 8–10. The experimental results based on the proposed methodology are shown in Figures 11–13. From Figures 9 and 12, we can see that the x and y position errors based on the proposed methodology are less than those based on closed-loop

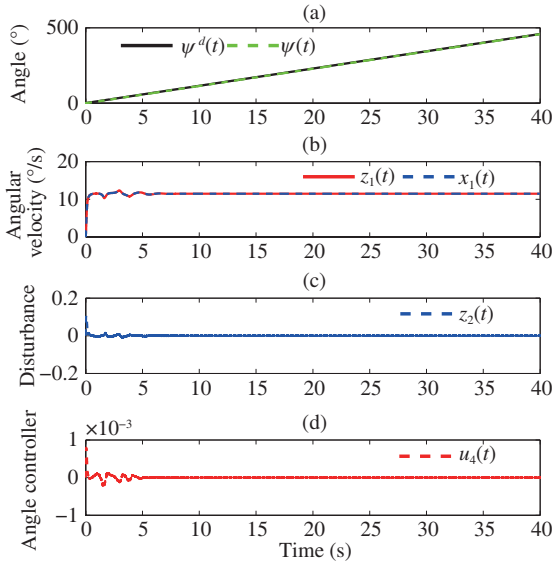


Figure 6 (Color online) Yaw angle tracking results of two-dimensional position simulation. (a) Yaw angle; (b) yaw angular velocity; (c) yaw angle disturbance estimation; (d) yaw angle controller.



Figure 7 (Color online) The experimental quadrotor platform.

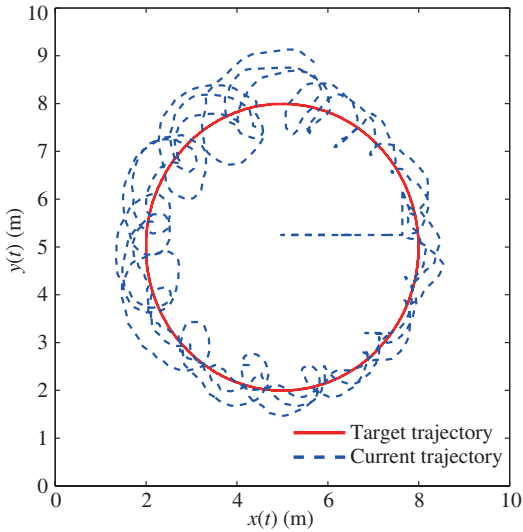


Figure 8 (Color online) Two-dimensional position experimental results of a quadrotor based on the dual closed-loop PID attitude controller.

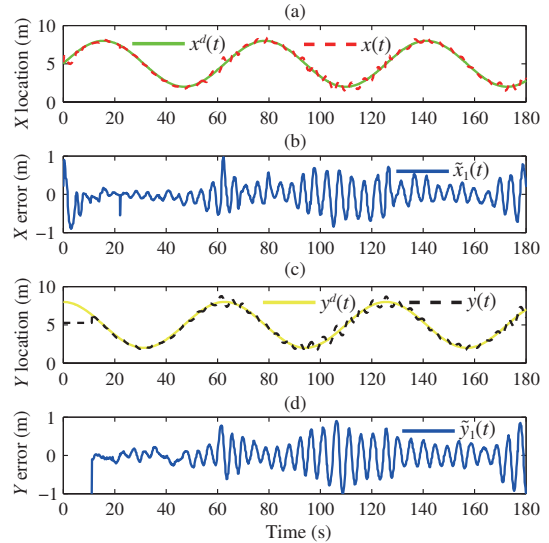


Figure 9 (Color online) Trajectory tracking experimental results based on the dual closed-loop PID attitude controller. (a) x position; (b) x position error; (c) y position; (d) y position error.

PID attitude controller. From Figures 8 and 11, it is apparent that the current trajectory of quadrotor based on the proposed methodology is smoother than that obtained by the PID attitude controller. The Figures 10 and 13 are local enlarged plots of the roll angle, which also illustrate that the proposed methodology is more favorable. Figures 13(b) and (c) show the angular velocity and disturbance tracking results of ESO (16) and (17). It is easy to see that the $z_1(t)$ of ESO tracks the location $x(t)$ quickly and accurately and $z_2(t)$ provides the estimate of disturbance.

6 Conclusion

In this paper, a position controller for quadrotors has been put forward based on trigonometric saturation function. Additionally, an attitude controller with dual closed-loop control structure has been designed.

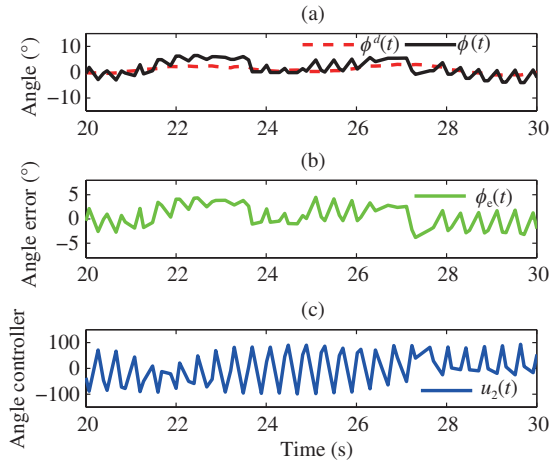


Figure 10 (Color online) Roll angle tracking experimental results based on the dual closed-loop PID attitude controller. (a) Roll angle; (b) roll angle error; (c) the input of roll angle controller.

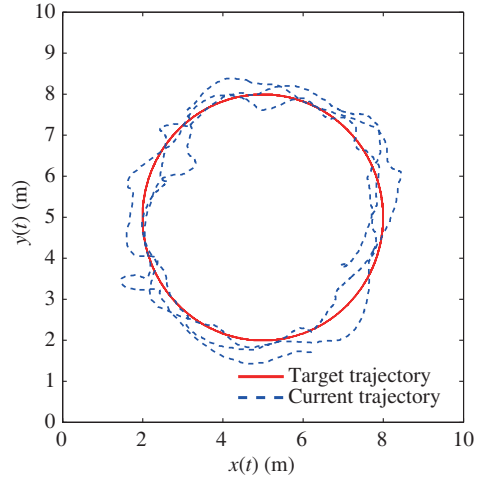


Figure 11 (Color online) Two-dimensional position experimental results of a quadrotor based on the proposed method.

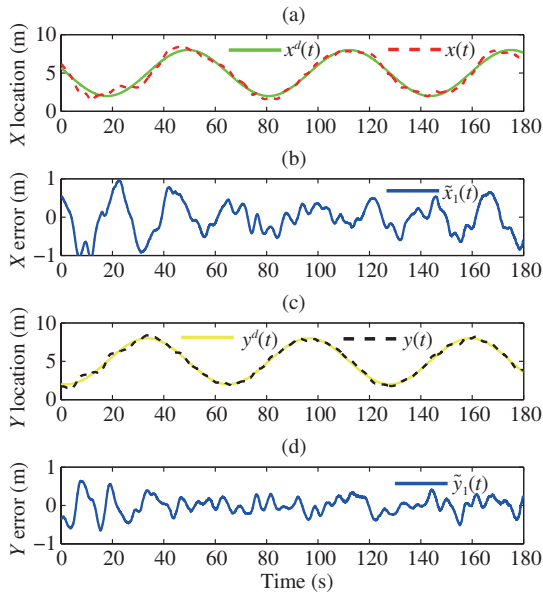


Figure 12 (Color online) Trajectory tracking experimental results based on the proposed method. (a) x position; (b) x position error; (c) y position; (d) y position error.

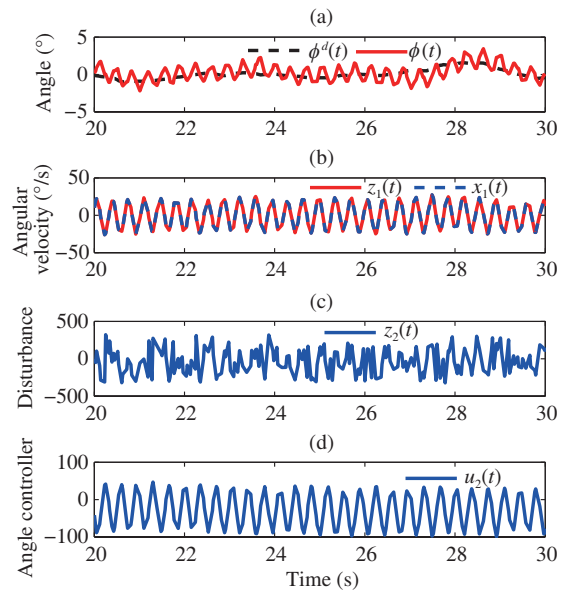


Figure 13 (Color online) Roll angle tracking experimental results based on the proposed method. (a) Roll angle; (b) roll angular velocity; (c) roll angle disturbance estimation; (d) the input of roll angle controller.

The external disturbance and unmodeled dynamics has been estimated and then compensated by the composite control scheme. Some sufficient conditions have been provided to guarantee the stability of the ESO and the closed-loop control system. The simulation and practical experimental results have demonstrated the effectiveness and advantage of the proposed method. One of the possible future research directions would be the study of multi-quadrotor subjected to communication networks [31–34].

Acknowledgements This work was supported in part by Royal Society of the U.K., in part by Research Fund for the Taishan Scholar Project of Shandong Province of China, in part by National Natural Science Foundation of China (Grant No. 61503001), and in part by Alexander von Humboldt Foundation of Germany.

References

- 1 Tousi M M, Khorasani K. Optimal hybrid fault recovery in a team of unmanned aerial vehicles. *Automatica*, 2012, 48: 410–418
- 2 Gandolfo D C, Salinas L R, Brandao A, et al. Stable path-following control for a quadrotor helicopter considering energy consumption. *IEEE Trans Control Syst Technol*, 2017, 25: 1423–1430
- 3 Cabecinhas D, Naldi R, Silvestre C, et al. Robust landing and sliding maneuver hybrid controller for a quadrotor vehicle. *IEEE Trans Control Syst Technol*, 2016, 24: 400–412
- 4 Loianno G, Brunner C, McGrath G, et al. Estimation, control, and planning for aggressive flight with a small quadrotor with a single camera and IMU. *IEEE Robot Autom Lett*, 2017, 2: 404–411
- 5 Dong X W. *Formation and Containment Control for High-Order Linear Swarm Systems*. Berlin: Springer, 2015
- 6 Liang X, Fang Y C, Sun N, et al. Nonlinear hierarchical control for unmanned quadrotor transportation systems. *IEEE Trans Ind Electron*, 2018, 65: 3395–3405
- 7 Aguiar A P, Hespanha J P. Trajectory-tracking and path-following of underactuated autonomous vehicles with parametric modeling uncertainty. *IEEE Trans Autom Control*, 2007, 52: 1362–1379
- 8 Cao N, Lynch A F. Inner-outer loop control for quadrotor UAVs with input and state constraints. *IEEE Trans Control Syst Technol*, 2016, 24: 1797–1804
- 9 Wang X H, Shirinzadeh B, Ang M H. Nonlinear double-integral observer and application to quadrotor aircraft. *IEEE Trans Ind Electron*, 2015, 62: 1189–1200
- 10 Yuan Y, Yuan H H, Wang Z D, et al. Optimal control for networked control systems with disturbances: a delta operator approach. *LET Control Theory Appl*, 2017, 11: 1325–1332
- 11 Yuan Y, Wang Z D, Guo L. Event-triggered strategy design for discrete-time nonlinear quadratic games with disturbance compensations: the noncooperative case. *IEEE Trans Syst Man Cybern Syst*, 2018, 48: 1885–1896
- 12 Leena N, Saju K K. Modelling and trajectory tracking of wheeled mobile robots. *Procedia Tech*, 2016, 24: 538–545
- 13 Sun W C, Tang S Y, Gao H J, et al. Two time-scale tracking control of nonholonomic wheeled mobile robots. *IEEE Trans Control Syst Technol*, 2016, 24: 2059–2069
- 14 Xu B. Disturbance observer-based dynamic surface control of transport aircraft with continuous heavy cargo airdrop. *IEEE Trans Syst Man Cybern Syst*, 2017, 47: 161–170
- 15 Kim W, Shin D, Won D, et al. Disturbance-observer-based position tracking controller in the presence of biased sinusoidal disturbance for electrohydraulic actuators. *IEEE Trans Control Syst Technol*, 2013, 21: 2290–2298
- 16 Pereira P O, Cunha R, Cabecinhas D, et al. Leader following trajectory planning: a trailer-like approach. *Automatica*, 2017, 75: 77–87
- 17 Tayebi A, McGilvray S. Attitude stabilization of a VTOL quadrotor aircraft. *IEEE Trans Control Syst Technol*, 2006, 14: 562–571
- 18 Meng Z Y, Ren W, You Z. Distributed finite-time attitude containment control for multiple rigid bodies. *Automatica*, 2010, 46: 2092–2099
- 19 Tian B L, Liu L H, Lu H C, et al. Multivariable finite time attitude control for quadrotor UAV: theory and experimentation. *IEEE Trans Ind Electron*, 2018, 65: 2567–2577
- 20 Shi X N, Zhang Y A, Zhou D. A geometric approach for quadrotor trajectory tracking control. *Int J Control*, 2015, 88: 2217–2227
- 21 Liu H, Xi J X, Zhong Y S. Robust attitude stabilization for nonlinear quadrotor systems with uncertainties and delays. *IEEE Trans Ind Electron*, 2017, 64: 5585–5594
- 22 Xia Y Q, Liu B, Fu M Y. Active disturbance rejection control for power plant with a single loop. *Asian J Control*, 2012, 14: 239–250
- 23 Han J Q. From PID to active disturbance rejection control. *IEEE Trans Ind Electron*, 2009, 56: 900–906
- 24 Wu D, Chen K. Frequency-domain analysis of nonlinear active disturbance rejection control via the describing function method. *IEEE Trans Ind Electron*, 2013, 60: 3906–3914
- 25 Guo B Z, Zhao Z L. On convergence of the nonlinear active disturbance rejection control for MIMO systems. *SIAM J Control Optim*, 2013, 51: 1727–1757
- 26 Chen S, Xue W, Zhong S, et al. On comparison of modified ADRCs for nonlinear uncertain systems with time delay. *Sci China Inf Sci*, 2018, 61: 070223
- 27 Bai W Y, Xue W C, Huang Y, et al. On extended state based Kalman filter design for a class of nonlinear time-varying uncertain systems. *Sci China Inf Sci*, 2018, 61: 042201
- 28 Liu G P, Shi P, Han J, et al. Active disturbance rejection control for uncertain multivariable systems with time-delay. *IET Control Theory Appl*, 2007, 1: 75–81
- 29 Cabecinhas D, Cunha R, Silvestre C. Experimental validation of a globally stabilizing feedback controller for a quadrotor aircraft with wind disturbance rejection. In: *Proceedings of American Control Conference, Washington, 2013*. 1024–1029
- 30 Yang H J, Cheng L, Xia Y Q, et al. Active disturbance rejection attitude control for a dual closed-loop quadrotor under gust wind. *IEEE Trans Control Syst Technol*, 2018, 26: 1400–1405
- 31 Yuan Y, Wang Z D, Zhang P, et al. Nonfragile near-optimal control of stochastic time-varying multiagent systems with control- and state-dependent noises. *IEEE Trans Cybern*, 2018. doi: 10.1109/TCYB.2018.2829713
- 32 Yuan Y, Wang Z D, Zhang P, et al. Near-optimal resilient control strategy design for state-saturated networked systems under stochastic communication protocol. *IEEE Trans Cybern*, 2018. doi: 10.1109/TCYB.2018.2840430
- 33 Liu J L, Liu Q H, Cao J, et al. Adaptive event-triggered H_∞ filtering for T-S fuzzy system with time delay. *Neurocomputing*, 2016, 189: 86–94
- 34 Liu J L, Cao J, Wu Z A, et al. State estimation for complex systems with randomly occurring nonlinearities and randomly missing measurements. *Int J Syst Sci*, 2014, 45: 1364–1374